Rapid synthesis of trimetallic alloy PtPdNi nanosponges: structural, morphology and catalytic performance

M. A. Abdul Razak[a], M. D. Johan Ooi[a,b,*], Y. Yusof[a], P. R. Jubu[c]
[a]*Nano-Optoelectronic Research and Technology Laboratory, School of Physics, Universiti Sains Malaysia, 11800 Minden, P. Pinang, Malaysia*
[b]*Energy Laboratory, School of Physics, Universiti Sains Malaysia, 11800 Minden, P. Pinang Malaysia*
[c]*Department of Physics, University of Agriculture Makurdi, P.M.B. 2373, Makurdi, Benue State, Nigeria*

Pt alloy nanostructures have been explored as promising anode catalysts for methanol oxidation reaction. However, the Pt catalyst have continued to face challenges that are yet to be resolved. Studies have shown that the size and geometric structure can influence a material's catalytic activity and is related to the synthesis technique. In this study, PtPdNi nanostructures were produced at different synthesis duration. FESEM results show that all the samples exhibited nanosponges structure. The PtPdNi synthesized for 150 s, exhibited higher catalytically active toward methanol oxidation and resistance to carbon monoxide poisoning.

1. Introduction

One of the most promising alternatives for power generation is the direct methanol fuel cell. It is an electricity-generating method that converts methanol directly into electrical energy. Without a reformer, the liquid chemical fuel is fed directly into the reactor to operate direct methanol fuel cells (DMFC) [1]. The system is compact and suitable for portable and mobile power generation. Since methanol is safe for storage and transportation, DMFC have been studied and widely used. DMFC exhibit fast anodic reactions, which have been viewed as clean and highly efficient new-generation energy conversion devices [2]. However, their extensive use has been constrained by the high cost of the precious metal (often Pt) and the risk of carbon monoxide poisoning. To accelerate the commercialisation of DMFC, high-activity, durable electrocatalysts for methanol oxidation are sought. The poor reactant action has limited the use of the existing methanol electrooxidation catalyst, which is far from expectation. Methanol oxidation reaction's (MOR) slow kinetics and the device's high price are two additional drawbacks. To aid in the commercialisation of the DMFC, an active, long-lasting, affordable, and high-performance catalyst for the MOR process must be designed and developed [3]. Some progresses have been accomplished by synthesising Pt alloys and non-platinum catalysts with various-shaped nanostructures to weaken the Pt - CO interactions.

Among the metals, Pt is the most favoured electrocatalyst. However, it has some demerits in exhibiting low activity for methanol oxidation in alkaline solution due to its inability to adsorb suitable oxygen-containing species in potential regions of methanol adsorption [4]. The second and third metals have been proposed as cocatalysts to solve this issue. Although adding the second and third metals improves the catalytic activity to some extent, optimising the anode's reaction kinetics is essential to make the DMFC commercially viable. As for Pt catalyst, alloying it with other noble metals such as Pd [5], Au [6], Ag [7], or 3d transition metals such as Fe [8], Ni [9], Co [10], and Cu [11], have been revealed as a practical approach toward developed oxygen reduction

---

reaction (ORR) electrocatalysts. In the case of Pt and Pt-based catalysts, fundamental studies of well-defined extended surfaces have shown that the enhanced catalytic reactivity develops from the modified electronic structures of Pt in these alloy catalysts, which reduces the absorption of oxygen spectator species such as OH⁻. Pd can reduce protons, store, and release hydrogen, and is also used to remove adsorbed CO formed from the methanol electrooxidation, thus lessening the poisoning effect. The release of hydrogen by Pd may thus provide a viable route for lowering the surface concentration of adsorbed CO, permitting the continual oxidation of organic molecules at the Pd surface. A combination of Pt and Pd will change the catalysts' electronic structures, which may help reduce poisoning by oxidising CO to CO_2 [4]. The atomic radius of Pt is like that of Pd (0.138 and 0.137 nm), so the substitution of Pt with Pd atoms expands the lattice only slightly, and Pt-Pd alloy is found to bear the face-centered cubic structure. Stamenkovic et al. [12] reported the use of Pt_3Ni (111) as a high-performance catalyst. The surface of Pt_3Ni (111) is rich in Pt, and the subsurface is rich in Ni. This structure reduces the d-band centre by 0.34 eV, which weakens the adsorption of oxygen-containing substances by Pt atoms on the surface, thereby revealing more active sites for further oxygen adsorption and reactions. Experimental results show that the activity of Pt_3Ni (111) is ten times higher than that of Pt (111), which is 90 times higher than that of commercial Pt-C catalyst [13]. Wu et al. [14] reported the preparation of octahedral, truncated octahedral, and cubic shapes PtNi. Despite possessing interesting electrocatalytic properties, PtPd and PtNi have been less extensively studied for fuel cell applications than Pt.

Nanoparticles (NP) have gained attention in technological developments because of their physicochemical properties, such as catalytic activity, light absorption, melting point, durability, and electrical and thermal conductivity, which surpass their bulk counterparts [15]. There are two methods to synthesise NP, which are bottom-up and top-down. The bottom-up method includes colloidal, micro-emulsion, sonochemical, hydrothermal, and chemical bath deposition, is preferred in the synthesis of NP over the top-down approach due to low impurities, homogenous chemical composition, simple set-up, cheaper, operating at low reaction temperatures (<350 ºC) and the parameters is easy to control. The bottom-up method required suitable metal salt precursors or coordinated metals via suitable ligands. Among the bottom-up approach, the chemical reduction is popular in producing noble trimetallic NP such as PtPdNi by reducing noble metal ions to zero-valent atoms [16]. The synthesis of PtPdNi highly depends on the reaction time, solvent, temperature, ligand effects, capping agent, and reducing agent. This technique can operate in organic or inorganic solvents and at room temperature. The reducing agent assists in producing the growth species, while the capping agent stabilises the NP against aggregation [17]. The most common reducing agents are sodium borohydride [18], sodium citrate [19], and ascorbic acid [20]. In contrast, capping agents such as PVP, PVA, and PEG exhibit ligand effects that can stabilise and affect the size and shape of the nanoparticle.

Trimetallic nanoparticles are made up of three different metals that are alloyed together. In both industrial and scientific terms, trimetallic and bimetallic nanoparticles are garnering more attention than monometallic since the catalytic properties of trimetallic can be adjusted better than those of a single monometallic substance [21]. On the other hand, trimetallic nanoparticles have an unstable surface area, necessitating stabilisers such as block copolymers, organic ligands, surfactants, and dendrimers to minimise their high surface energy [21]. Li et al. successfully synthesised trimetallic PtPdNi mesoporous nanoparticles in a high yield in the presence of Pluronic F127 as a surfactant and ascorbic acid as a reducing agent at a mild reaction temperature of 40 ºC. They observed that surfactant F127 serves as a pore-shaping agent for the generation of mesoporous structure. With their structural (i.e., highly mesoporous and highly open structures) and compositional (i.e., ternary alloy) advantages, the as-synthesised PtPdNi exhibit enhanced ORR activity relative to PtPdNi nanodendrites, PtPd mesoporous nanoparticles and Pt/C catalysts [16].

Zhai et al. [22] have developed a facile, rapid, and surfactant-free method to synthesise ternary PtPdNi alloy nanoarchitecture within 5 min, which shows extremely high performance in methanol electrooxidation reaction. They compare the catalytic activity of the as-synthesised PtPdNi with its components, and they found that the PtPdNi catalyst shows higher activity than Pt, PtPd and PtNi, and 3.58 times higher than commercial Pt black in Pt-based mass activity. All the methods reported to date do not investigate the effect of synthesis time/ duration to understand the

growth and the formation of PtPdNi nanostructures. Since the use of stabilisers and capping agent tend to block the nanoparticle's active surface area, resulting in a reduction in catalytic activity. Thus, nanostructures synthesised without stabilisers and capping agents are most desired [22].

In this study, PtPdNi are synthesised using a, rapid, one-step reduction method by mixing three metallic precursors under different synthesis duration. The prepared PtPdNi nanoparticles are analysed using Field Emission Scanning Electron Microscopy (FESEM), Energy Dispersive X-ray (EDX) spectroscopy, X-ray diffraction (XRD), and cyclic voltammetry (CV) measurements. FESEM is used to study the surface morphologies, EDX for determining the elemental composition, XRD for structural analysis, and CV measurements to investigate their performances in the methanol oxidation reaction.

2. Experimental

Hexachloroplatinic acid (H_2PtCl_6), Tetrachloropalladic acid (H_2PdCl_4), Nickel chloride ($NiCl_2$), Sodium borohydride ($NaBH_4$), Methanol and Nafion® 5 wt% were purchased from Sigma Aldrich. Hydrochloric acid (HCl), Nitric acid (HNO_3) and Hydroflouric acid (HF) were purchased from Q Rec. All chemicals were used as obtained without further purification. In the preparation of PtPdNi trimetallic alloy,1.6 mL of 0.02 M of H_2PdCl_4, 4.8 mL of 0.02 M of H_2PtCl_6, and 1.6 mL of 0.02 M $NiCl_2$ were mixed in a beaker. 0.5 mL of $NaBH_4$ was added to the solution and stirred for the reaction. The yellowish solution turned into a black product, indicating that the $NaBH_4$ successfully reduced the metal salts into the PtPdNi trimetallic alloy. This sample is labelled as an instant reaction in a duration of 0 s. The experiment was repeated by varying the synthesis time for 30, 60, 90, 120, and 150 s. All the products were collected and centrifuged at 7500 rpm for 15 minutes to remove the unwanted products. The product was re-dispersed and washed three times in deionised water. The samples were ultrasonicated to re-disperse the products before characterisation.

The morphology of the samples was characterised using a field emission scanning electron microscope (FESEM) (NOVA Nanosem 45 operated at the acceleration voltage of 5 kV. Energy-dispersive X-ray spectroscopy (EDX) equipped with FESEM was used to determine the elemental composition of the synthesised samples. The structural properties were analyzed using an X-Ray diffractometer (XRD) (PANalytical X'PERT PRO MRD PW 3040/60 operating at a wavelength of 1.5418 Å by CuKα radiation. The catalytic performance of the synthesised PtPdNi was analyzed via cyclic voltammetry measurements using eDAQ (ER466) Integrated Potentiostat. The latter process incorporated a three-electrode system with glassy carbon as the working electrode, Pt rod as the counter electrode, and saturated calomel electrode (SCE) as the reference electrode. The working electrode was prepared by drop-casting a 5 μL PtPdNi sample (with a loading of 10 μg) on the glassy carbon electrode (Ø = 3.0 mm, surface area of 0.07 cm^2), which has been polished with γ-Al_2O_3 (0.3 and 0.05 μm) before use and dried under N_2 flow. Nafion® (0.05 wt.%, 5 μL) solution was dropped wise onto the PtPdNi film and dried at room temperature before the electrochemical measurements were performed. The electrolytes for electrochemical testing were deaerated throughout the measurements with high-purity N_2 gas. The Pt-O and Pd-O reduction process was analyzed using cyclic voltammetry in 10 mL of 1 M NaOH electrolyte, with a potential sweep rate of 50 mV/s and a scanning potential between 0 V and 1.0 V vs SCE. Methanol oxidation was studied for 20 cycles by adding 10 mL of 1 M methanol (MetOH) in 10 mL of 1 M NaOH at 0 V and 1.0 V vs SCE.

3. Results and discussions

Fig. 1 demonstrates the FESEM results for the PtPdNi samples prepared at various synthesis times. Notably, no extra capping agent was applied during the synthesis procedure. At 100k times magnification (scale: 500 nm), it is observed that all samples are composed of an open interconnected network backbone with several small pores embedded within it, forming nanosponges structures. The nanosponges are small, less than one micrometre-diameter structures

that resemble small meshes. They have pores size about 1-2 nm in diameter and are made up of tiny nanoparticles linked together to form skeletons. The nanosponges' structure is probably due to the formation of Pt-Pd and Pt-Ni. The FESEM images of the PtPdNi synthesised at different reaction times show a minor change in particle size. The estimated average particle size is about 10 - 80 nm, measured via Image J software. There are no changes in shape, probably because of the use of a small amount of reducing agent throughout the synthesis. As is well known, the reducing agent plays a role in the formation and growth of PtPdNi nanoparticles.
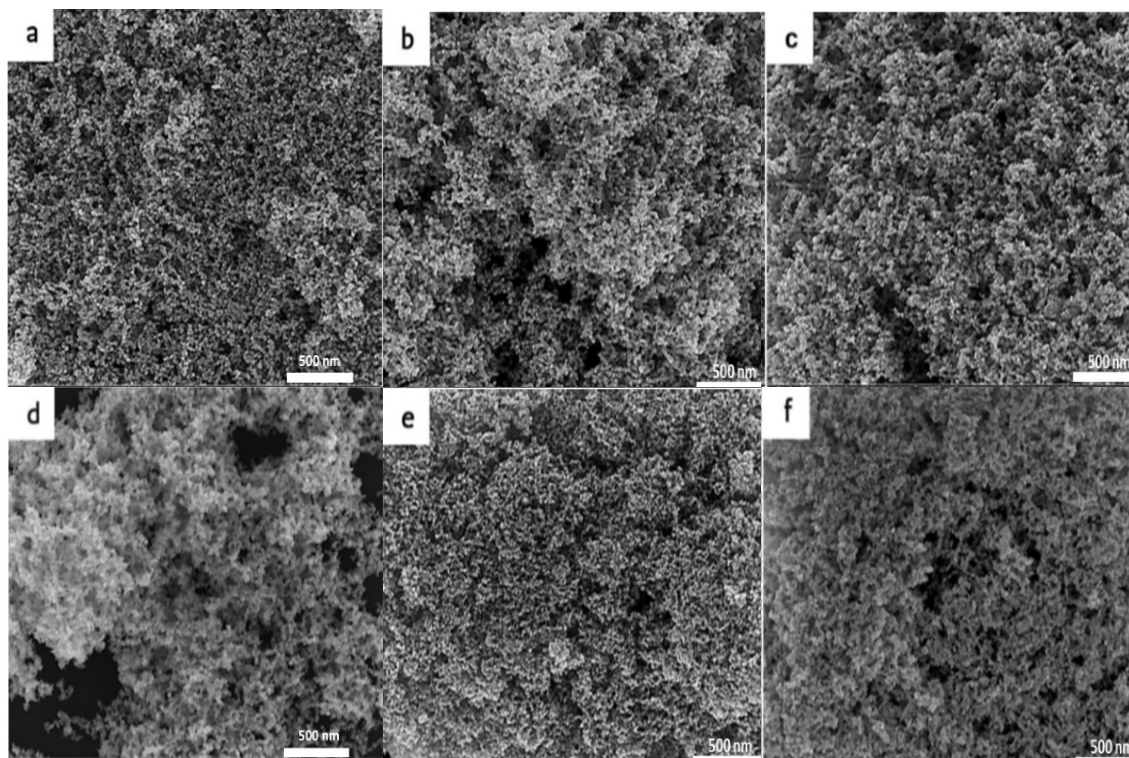
Fig. 1. FESEM image of the synthesised PtPdNi nanoparticles at different synthesis duration: a) 0 s, b) 30 s, c) 60 s, d) 90 s, e) 120 s, and f) 150 s.

The literature report that the size, shape, and structure of trimetallic nanoparticles, as well as the distribution of their elements, will determine their attributes. Therefore, the elemental composition of the prepared PtPdNi nanoparticles was determined using EDX (Fig. 2). The EDX spectrum of the PtPdNi synthesised at 0 s (Fig. 2a) shows the presence of Pt and Ni elements. The presence of Pt is more prominent during synthesis at an instant time than Ni, indicating that Pt salt was first reduced, followed by Ni salt. Upon increasing the synthesis time from 30 to 150 s (Fig. 2b), the EDX results for the five samples show the existence of the Pd element along with Pt and Ni, which is an indication that Pd salt is difficult to be reduced and requires at least 30 s to form zero-valent. The appearance of Si elements in all the samples is mainly because the Si wafer was used as a substrate to support the films. Meanwhile, a small amount of C element was detected probably because of the carbon tape used to seal and attach the analysed samples.
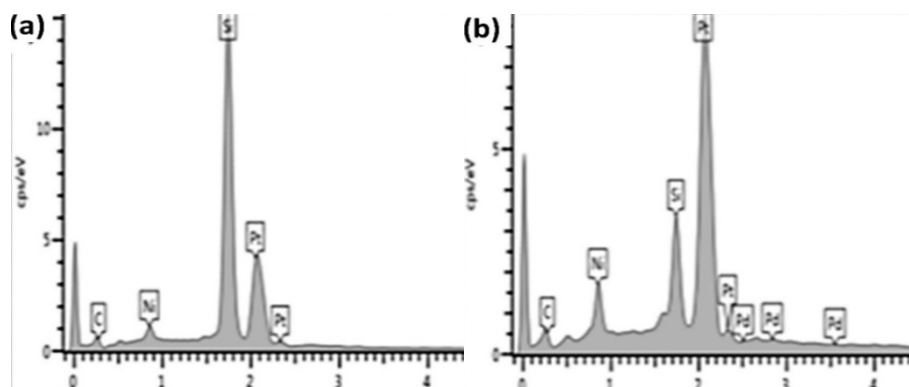
Fig. 2. EDX spectral of the PtPdNi prepared at different synthesis times: a) 0 s, b) 30 s to 150 s.

The proposed chemical reaction is given in Eq. 1

$$H_2PtCl_6 + H_2PdCl_4 + NiCl_2 \rightarrow PtPdNi + 2H_2 + 6\,Cl_2 \tag{1}$$
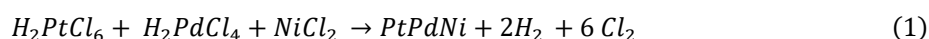
PtPdNi nanosponges were reduced from the metal precursors assisted by a reducing agent, NaBH$_4$. Chemical reduction methods typically use a suitable reducing agent until it reaches the zero-valent phase and produces bimetallic or trimetallic alloy nanoparticles. For the above reaction, H$_2$PtCl$_6$, H$_2$PdCl$_4$ and NiCl$_2$ were the metal precursor reduced by NaBH$_4$. Because the reduction process follows the electronegativity table, the Pt (II) precursor, was reduced first, yielding Pt (0) nanoparticles, followed by the reduction of Ni (II) and Pd (II) precursor, resulting in Ni (0) and Pd (0). Without using a template or surfactant, the production of PtPdNi nanostructures might be explained as the self-assembly of the three metals in deionised water, with the reduced metals stabilised due to a decrease in interfacial energy.

The formation of a non-ordered porous structure mainly depends on the reduction rates. It has been established that the reducing power of reductant, the type of solvent, and counter-ion metal salt affect the formation of nuclei [23]. The metal ion reduced by NaBH$_4$ could occur instantaneously since a strong reducing agent was used. The large numbers of nuclei form the nanoparticles, which are the primary units of the network, followed by spontaneous destabilisation. Subsequently, the fusion and growth of metal nanoparticles led to a three-dimensional interconnected backbone. The solvent's dielectric constant and high ionic strength also help the colloidal particles overcome the repulsion barrier and coalescence with one another. During this process, NaBH$_4$ gets hydrolysed, resulting in the formation of hydrogen gas bubbles which act as dynamic templates to generate pores within the agglomerates leading to the formation of hollow structures [23].

Fig. 3 shows the XRD results which reveal the crystalline structures and phase purity of synthesised the PtPdNi prepared at different reaction times. The XRD patterns for all samples showed broad peaks and are not weak, indicating their low crystalline nature. All samples presented four diffraction peaks centered at Bragg angles of about 40.2°, 46.7°, 68.1° and 82.0° corresponding to the planes (111), (200), (220), and (311) of platinum and palladium face-centered cubic (fcc) lattice structure [24]. These diffraction peaks are shifted with respect to the reflections of bulk Pt (JCPDS card no. 01-087-0640) and Pd (JCPDS card no. 01-087-0645), suggesting a solid solution formation between the metals [25- 26]. Furthermore, the X-ray patterns does not show any visible peak related to the fcc arrangement of bulk Ni (JCPDS card no. 00-004-0850). The lattice mismatch between the three metals also contributes, to some extent, to the contraction of the Pt fcc lattice [27]. It is to be noted that the diffraction angle for Pt and Pd are very close to each other. Moreover, the diffraction peaks of the alloys containing Ni were slightly shifted toward higher two theta values from the standard Pt, indicating shrinkage of lattice spacing due to the incorporation of smaller Ni into the lattice of Pt or Pd [28]. The smaller size and the same valence states of Ni as that of Pd and Pt allow Ni to be incorporated into either Pd or Pt or Pt-Pd bimetallic system [28].

The Scherrer equation (Eq. 2)[29] was used to estimate the crystallite size of the synthesised PtPdNi samples at different reaction times.

$$D = \frac{(k \times \lambda)}{(\beta \times cos\,\theta)} \qquad (2)$$

where D is the crystallite size in nm, k refers to Scherrer constant (0.9), λ is the wavelength of X-rays (1.5406 Å), and β is full width at half maxima corresponding to the (111) plane, and θ is the Bragg diffraction angle in degree. The estimated crystallite sizes for the PtPdNi catalysts with different reaction times are presented in Table 1.
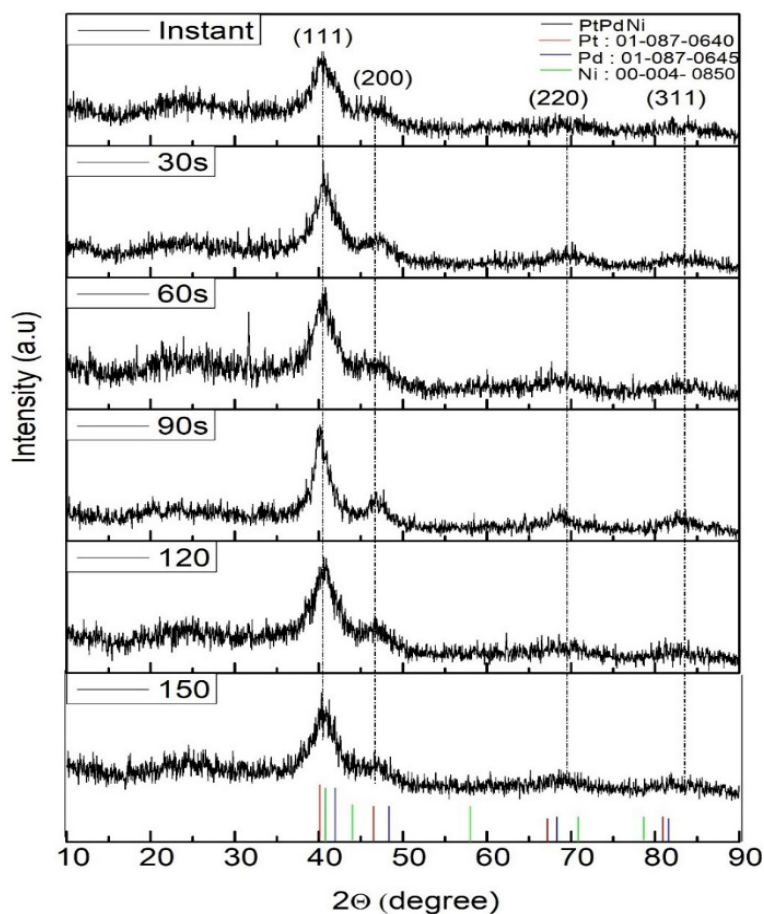
Fig. 3. XRD patterns of the PtPdNi synthesised at different reaction duration.

Table 1. The average crystallite size measurement of the samples prepared at different synthesis times.

Synthesis time (s)	2Θ (degree)	FWHM ($\times 10^{-3}$) radian	D, crystallite size (nm)
0	40.59	31.59	4.68
30	40.53	26.00	5.68
60	40.80	29.30	5.05
90	40.20	27.80	5.31
120	40.90	30.90	4.78
150	40.36	18.32	8.07

Table 1 illustrate that increasing the reaction time induced the formation of bigger crystallite sizes. As such, the PtPdNi that produced for the duration of 0 s exhibits the smallest

crystallite size compared to other samples, which may be due to the low degree of nucleation and growth rate of nanoparticles [30]. Prolonging the reaction time promoted solvent evaporation and maintained the solution in a supersaturation state, leading to increased crystallite size.

CV profiles of the synthesised PtPdNi trimetallic alloy nanosponges are shown in Fig. 4. The oxide production and reduction processes are represented by the measured CV profiles of PtPdNi taken at the scan rate of 50 mV s^{-1} in 1 M NaOH electrolyte. During the forward scan, the oxidation of Pt/Pd for the instant (0 s) sample happens at a higher potential, which can be seen around 0.4 V vs. SCE, potentially generating surface oxides. During the reverse scan, the produced oxide is reduced in the potential range of 0.2 to 0.4 V vs. SCE, which are the typical maxima for Pt and Pd-based materials [31].
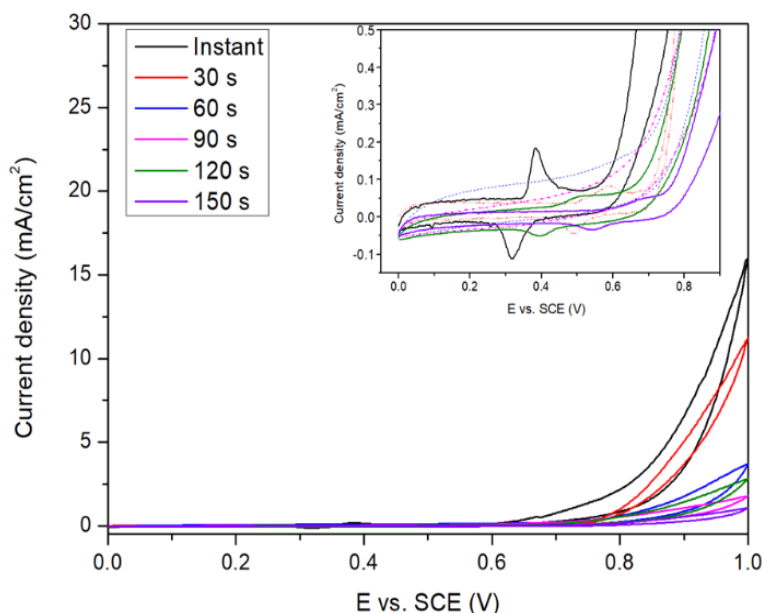
Fig. 4. The CV profiles of the PtPdNi at different reactions time.

The charge generated during the reduction process of PtO and PdO was used to calculate the effective catalytic surface area (ECSA) of the synthesised PtPdNi electrocatalysts. Eq. 3 is used to calculate the ECSA of all these electrocatalysts.

$$ECSA = \frac{Q_H}{SL}$$ (3)

where Q_H is the Coulombic charge required to reduce oxide layers such as PtO and PdO, S is the proportionality constant used to relate charges with the area, and L is the catalyst loading in g, which in this experiment is 10 µg. The charge needed to reduce PdO and PtO monolayer is assumed to be 405 µCcm^{-2} and 420 µCcm^{-2}, respectively [32]. The mean value of charge required for oxide reduction was computed for the Pt-Pd/C catalyst with a Pt to Pd ratio of 1: 2 as 410 µCcm^{-2} and used in the ECSA calculation for the alloyed catalyst, PtPdNi. Table 2 shows the value of ECSA of PtPdNi alloyed catalyst at different reaction times.

Table 2. ECSA value for the PtPdNi catalyst with different times of reaction.

Synthesis time (s)	Q_H (mC cm^{-2})	ECSA (cm^2/g)
0	46.28 x 10^{-4}	79.02
30	24.73 x 10^{-4}	42.22
60	2.15 x 10^{-4}	3.66
90	0.26 x 10^{-4}	0.44
120	9.41 x 10^{-4}	16.06
150	10.72 x 10^{-4}	18.30

The highest ECSA value obtained is from the PtPdNi synthesis under instant reaction time (79.02 cm^2/g), which is 4.3 times higher than the ECSA value of the sample synthesised for the highest reaction time of 150 s (18.30 cm^2/g). The high ECSA value implies that the PtPdNi reduced by NaBH$_4$ at 0 s is more active toward hydroxide adsorption and desorption, probably due to the high surface area of the small particle and uniform dispersion. The ECSA value of the samples produced for 60 and 90 s are much smaller than the instant (0 s) reaction, probably due to the low density compared to the instant sample. For pure Pt, the atomic distance of Pt-Pt is not the optimum spacing, while the alloying of Pd and Ni to Pt metal leads to decreasing nearest-neighbour distance. Hence, foreign atoms of Pd and Ni may aid oxygen dissociation and adsorption on the alloy surface, favouring the methanol oxidation reaction. In metal catalysts, adding two or three elements can improve monometallic catalysts' catalytic selectivity and activity.

Fig. 5 demonstrates the CV profiles of the synthesised PtPdNi catalysts toward methanol oxidation. The inset figure shows the CV profiles of Pt and Pd catalysts for comparison. During the CV scan, each catalyst showed two unique oxidation peaks. The methanol oxidation is related to the peak obtained in the forward scan (anodic). In contrast, the oxidation of carbonaceous species generated on the catalyst surface during the forward scan is associated with a weaker peak acquired in the reverse scan (cathodic). Fig. 6 depicts the magnified version of Fig. 5. The oxidation peak in the forward scan relates to the oxidation of chemisorbed species resulting from alcohol adsorption. The elimination of carbonaceous species generated during the oxidation of chemisorbed species in the forward scan is predominantly linked with the reverse scan peak. The reverse scan oxidation peak aids in regenerating active sites on the catalyst surface for subsequent oxidation reactions. Over different time reactions, the synthesised PtPdNi display various electrocatalytic performances toward methanol oxidation.
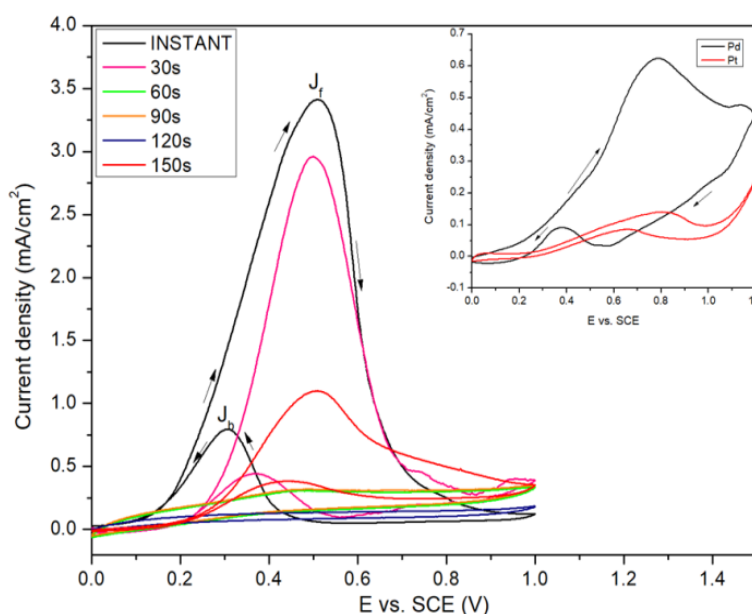
Fig. 5. CV curves of the PtPdNi catalyst with different time reactions in 1.0 M of methanol.
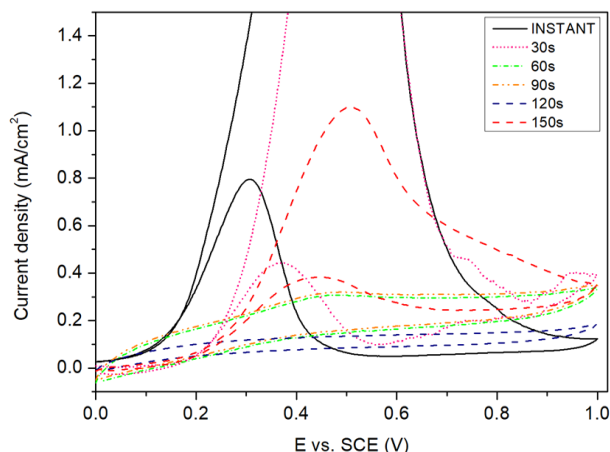
Fig. 6. Magnified CV curve of the PtPdNi electrocatalysts.

Fig. 6, showed that the CV profiles of the PtPdNi electrocatalysts synthesised at the instant reaction (0 s) exhibit the highest current peak in the forward scan, denoted as forward current, J_f. Also, this sample shows the highest current peak in the reverse scan, denoted as bias current, J_b. According to the literature, the J_b/J_f value of 1 indicates high methanol oxidation activity. The value of J_b and J_f for PtPdNi electrocatalysts at 0 s was 0.80 mA/cm^2 and 3.41 mA/cm^2, respectively. The sample prepared at 30 s exhibit J_b and J_f values of 0.44 mA/cm^2 and 2.96 mA/cm^2, respectively (Table 3). The value of the J_f and J_b for the samples produced at the durations of 60, 90, and 120 s are undefined (Fig. 6). For the sample reacted for 150 s, the value of J_b and J_f are 0.37 mA/cm^2 and 1.10 mA/cm^2, respectively.

The value of the ratio J_b/J_f that is close to 1 exhibits high methanol oxidation activity (Table 3). The J_b/J_f value for the sample reacted for 150 s was 0.34, which is the closest value to 1 compared to other samples. Although the ECSA value for the PtPdNi electrocatalyst was the highest at 0 s, the efficiency of methanol oxidation activity is the highest at 150 s, showing that the sample at 150 s was better at managing the carbon poisoning effect, which indicate higher resistant to carbon monoxide adsorption. Although samples prepared for 60, 90, and 120 s exhibit ECSA values, the J_f and J_b values are negligible, implying that the PtPdNi synthesised at 60, 90, and 120 s are catalytically active toward NaOH solution but inactive during the electrooxidation of methanol probably due to the high adsorption of carbon monoxide on the surface-active sites.

Table 3. The J_b and J_f values of PtPdNi electrocatalyst at different synthesis times.

Time (s)	J_b(mA/cm^2)	J_f (mA/cm^2)	J_b/J_f
0	0.80	3.41	0.20
30	0.44	2.96	0.15
60	-	-	-
90	-	-	-
120	-	-	-
150	0.37	1.099	0.34

4. Conclusions

PtPdNi nanosponges were successfully synthesised by a simple and rapid chemical reduction method using NaBH$_4$ as the reducing agent. The FESEM result shows that all samples exhibit nanosponges structures. EDX analysis shows that Pt, Pd, and Ni were present in the samples synthesised between the durations of 30 s to 150 s. Meanwhile, Pt and Ni elements were present at the instant (0 s) reaction. XRD result showed that all samples exhibit broad peaks and

typical fcc lattice structure. CV analysis showed that the sample prepared at the instant (0 s) exhibit a greater ECSA value which is (79.02 cm^2/g) compared to the monometallic Pt (13.53 cm^2/g) and Pd (9.65 cm^2/g), suggesting that the trimetallic alloy nanostructures exhibit better performance than the monometallic in catalytic activity. The PtPdNi sample synthesised for 150 s shows greater performance toward the electrooxidation of methanol. The J_b and J_f ratio value of synthesised PtPdNi reduced at 150 s is the highest indicating that the synthesised PtPdNi reduced at 150 s is better at managing the carbon poisoning effect.

References

[1] J.G Liu, T.S Zhao, R Chen, C.W Wong, Electrochemistry Communication 7 (3), 288 (2005); https://doi.org/10.1016/j.elecom.2005.01.011

[2] Z.A.C Ramli, S.K Kamarudin, Nanoscale Research Letter, 13 (1), 410 (2018); https://doi.org/10.1186/s11671-018-2799-4

[3] J.N Tiwari, R.N Tiwari, G Singh, K.S Kim, Nano Energy 2 (5), 553 (2013); https://doi.org/10.1016/j.nanoen.2013.06.009

[4] S.S Mahapatra, J Datta, International Journal of Electrochemistry 2011,563495 (2011); https://doi.org/10.4061/2011/563495

[5] J Wu, S Shan, H Cronk, F Chang, H Kareem, Y Zhao, J Luo, V Petkov, C.J Zhong, Journal of Physical Chemistry C 121 (26), 14128 (2017); https://doi.org/10.1021/acs.jpcc.7b03043

[6] S Yin, Y Ding, Dalton Transaction 49 (14), 4189 (2020); https://doi.org/10.1039/D0DT00205D

[7] Z Li, Y Li, C He, P.K Shen, Journal of Materials Chemistry A 5 (44), 23158 (2017); https://doi.org/10.1039/C7TA07525A

[8] Y Kim, A Anto Jeffery, J Min, N Jung, Nanomaterial 9 (10), 1491 (2019); https://doi.org/10.3390/nano9101491

[9] X Song, S Luo, X Fan, M Tang, X Zhao, W Chen, Q Yang, Z Quan, Frontier Chemistry 6, 468 (2018); https://doi.org/10.3389/fchem.2018.00468

[10] G Sievers, S Mueller, A Quade, F Steffen, S Jakubith, A Kruth, V Brueser, Journal of Power Sources, 268, 255 (2014); https://doi.org/10.1016/j.jpowsour.2014.06.013

[11] H.Y Kim, T Kwon, Y Ha, M Jun, H Baik, H.Y Jeong, H Kim, K Lee, S.H Joo, Nano Letter 20 (10), 7413 (2020); https://doi.org/10.1021/acs.nanolett.0c02812

[12] V.R Stamenkovic, B Fowler, B.S Mun, G Wang, P.N Ross, C.A Lucas, N.M Markovic, Science, 315 (80), 493 (2007); https://doi.org/10.1126/science.1135941

[13] J Zhang, H Yang, J Fang, S Zou, Nano Letter, 10 (2), 638 (2010); https://doi.org/10.1021/nl903717z

[14] Y Wu, S Cai, D Wang, W He, Y Li, Journal of American Chemical Society, 134 (21), 8975 (2012); https://doi.org/10.1021/ja302606d

[15] J Jeevanandam, A Barhoum, Y.S Chan, A Dufresne, M.K Danquah, Beilstein Journal of Nanotechnology 9, 1050 (2018); https://doi.org/10.3762/bjnano.9.98

[16] C Li, Y Xu, Y Li, H Yu, S Yin, H Xue, X Li, H Wang, L Wang, Green Energy Environmental 3 (4), 352 (2018); https://doi.org/10.1016/j.gee.2018.07.004

[17] K-H Huynh, X-H Pham, J Kim, S.H Lee, H Chang, W-Y Rho, B-H Jun, International Journal

of Molecular Sciences 21 (14),5174 (2020); https://doi.org/10.3390/ijms21145174

[18] A Morozan, A Dumitru, C Mirea, I Stamatin, F Nastase, A Andronie, S Vulpe, C Nastase, A Vaseashta, Functionalized Nanoscale Materials, Devices and Systems, Springer Netherlands, 445 (2008); https://doi.org/10.1007/978-1-4020-8903-9_46

[19] K Ranoszek-Soliwoda, E Tomaszewska, E Socha, P Krzyczmonik, A Ignaczak, P Orlowski, M Krzyzowska, G Celichowski, J Grobelni, Journal of Nanoparticle Research 19 (8), 273 (2017); https://doi.org/10.1007/s11051-017-3973-9

[20] T Xia, H Shen, G Chang, Y Zhang, H Shu, M Oyama, Y He, Journal of Nanomaterials 2014, 496249 (2014); https://doi.org/10.1155/2014/496249

[21] G Sharma, D Kumar, A Kumar, A.H Al-Muhtaseb, D Pathania, M Naushad, G.T Mola, 71,1216 (2017); https://doi.org/10.1016/j.msec.2016.11.002

[22] Y Zhai, Z Zhu, X Lu, Z Zhou, J Shao, H.S Zhou, ACS Applied Energy Materials 1 (1), 32 (2018); https://doi.org/10.1021/acsaem.7b00032

[23] S Ghosh, B. R Jagirdar, Chemistry Select 3 (25), 7184 (2018); https://doi.org/10.1002/slct.201801562

[24] J.J Arroyo-Gómez, D Barrera, R.M Castagna, J.M Sieben, A Alvarez, M.M.E Duarte, K Sapag, ChemCatChem 11 (15), 3451 (2019); https://doi.org/10.1002/cctc.201900291

[25] T Lopes, E Antolini, E.R Gonzalez International Journal of Hydrogen Energy 33 (20), 5563 (2008); https://doi.org/10.1016/j.ijhydene.2008.05.030

[26] G Fu, K Wu, J Lin, Y Tang, Y Chen, Y Zhou, T. Lu, The Journal of Physical Chemistry C 117 (19) 9826 (2013); https://doi.org/10.1021/jp400502y

[27] J Zhang, F.H.B Lima, M.H Shao, K Sasaki, J.X Wang, J Hanson, R.R Adzic The Journal of Physical Chemistry B 109 (48), 22701 (2005); https://doi.org/10.1021/jp055634c

[28] K Bhunia, S Khilari, D Pradhan ACS Sustainable Chemistry and Engineering 6 (6),7769 (2018); https://doi.org/10.1021/acssuschemeng.8b00721

[29] G Sreenivasa Kumar, N Ramamanohar Reddy, B Sravani, L Subramanyam Sarma, T Veera Reddy, V Madhavi, S Adinarayana Reddy Journal Cluster of Science 32, 27 (2021); https://doi.org/10.1007/s10876-019-01752-z

[30] H.S Wasly, M.S.A El-Sadek, M Henini Applied Physics A 124, 76 (2018); https://doi.org/10.1007/s00339-017-1482-4

[31] J Datta, A Dutta, S Mukherjee The Journal of Physical Chemistry C 115 (31), 15324 (2011); https://doi.org/10.1021/jp200318m

[32] R.N Singh, A Singh, Anindita. Electrocatalytic activity of binary and ternary composite films of Pd, MWCNT and Ni, Part II: Methanol electrooxidation in 1M KOH International Journal of Hydrogen Energy 34 (4), 2052 (2009); https://doi.org/10.1016/j.ijhydene.2008.12.047